An optimization of the local hall-petch relationship using slip trace analysis technique and scale transition rules: application in equiaxed ti-6al-4v titanium alloy

Fatna Benmessaoud, Mohammed Cheikh, Vincent Velay, Vanessa Vidal, Hiroaki Matsumoto

XV International Conference on Computational Plasticity. Fundamentals and Applications
COMPLAS 2019
E. Oñate, D.R.J. Owen, D. Peric, M. Chiumenti & Eduardo de Souza Neto (Eds)

AN OPTIMIZATION OF THE LOCAL HALL-PETCH RELATIONSHIP USING SLIP TRACE ANALYSIS TECHNIQUE AND SCALE TRANSITION RULES: APPLICATION IN EQUIAXED TI-6AL-4V TITANIUM ALLOY

FATNA. BENMESSAOUD*, MOHAMMED CHEIKH*, VINCENT. VELAY*, VANESSA. VIDAL*, HIROAKI. MATSUMOTO†,

* ICA, Toulouse University, CNRS, IMT Mines Albi, INSA, UPS, ISAE-SUPAERO
Campus Jarlard, 81013 Albi Cedex 09, France
e-mail: ica@mines-albi.fr, web page: http://www.mines-albi.fr/

† Department of Advanced Materials Science
Faculty of Engineering and Design Kagawa University
2217-20, Hayashi-cho, Kagawa 761-0396, Takamatsu, Japan
e-mail: matsu_h@eng.kagawa-u.ac.jp - Web page: https://www.kagawa-u.ac.jp

Key words: Multi-Scale Optimization, Ti-6Al-4V, Slip Trace Analysis, Scale Transition Rules, Critical Resolved Shear Stress (CRSS), Grain Size Effects.

Abstract. The aim of this work is to optimize the relative and the absolute Critical Resolved Shear Stress (CRSS) of slip mechanism in α-phase of Ti-6Al-4V titanium alloy. The influence of grain size is then modeled through a local Hall-Petch relationship. A slip trace analysis technique coupled with statistical reasoning were used to identify the CRSS ratios of basal $\langle a \rangle$, prismatic $\langle a \rangle$ and pyramidal $\langle c + a \rangle$ slip systems. The multi-scale transition rule of Berveiller-Zaoui was then used to determine the absolute CRSS in three different microstructures; Ti-6Al-4V with ultra fine grains (UFG), fine grains (FG) and standard grains (SD). Finally, the local Hall-Petch relationship was optimized. As expected, plastic deformation is mainly accommodated by prismatic and then basal slip systems. Due to their high CRSS, sliding in pyramidal systems is more difficult. Grain size shows a significant role on the activation of slip systems. By increasing the grain size, the CRSS of each slip system type decreases and thus sliding becomes easier in coarse grains.

1 INTRODUCTION

The multi-scale modeling of mechanical behavior of materials essentially requires to identify the local parameters. An accurate prediction of the material properties at different scales strongly depends on the local model formulation as well as the identification procedure of its parameters .

In Hexagonal Closed Packed (HCP) materials such as pure titanium, the plastic behavior is mainly accommodated by twinning and crystallographic sliding mechanisms. However, addition of some alloying elements such as aluminum limits the role of twinning mechanism [1–4] which is the case of Ti-6Al-4V alloy. In this alloy, three several types of slip systems namely basal $\langle a \rangle$, prismatic $\langle a \rangle$ and pyramidal $\langle c+a \rangle$ can accommodate the plastic strain. The Critical Resolved Shear Stress (CRSS) varies from a type to another [5]. Therefore, the identification of this parameter for titanium and its alloys remains difficult and only the relative values have been estimated in most of previous works [5–9]. Moreover, the CRSS not only depends on the HCP material (Ti, Zr, Mg ...) or the type of slip systems but also on the morphology features such as the grain size.

The present contribution aims to identify the CRSS of basal $\langle a \rangle$, prismatic $\langle a \rangle$ and pyramidal $\langle c+a \rangle$ slip systems types in three microstructures of Ti-6Al-4V titanium alloy. Hence, the Hall-Petch relationship can be optimized. In order to achieve this goal, a slip trace analysis technique was proposed to identify the slip systems by comparing their observed traces with those given by the theoretical rules. Then, a statistical methodology adapted from the work of Li et al. [6] was used to estimate the CRSS ratios. Finally, a multi-scale numerical optimization was proposed to determine the absolute CRSS and therefore the local Hall-Petch relationship.

2 OPTIMIZATION PROCEDURE

Four microstructures of an equiaxed Ti-6Al-4V reported in Tab.1 were used in the optimization procedure. T2-SD is characterized by a weak crystallographic texture and coarse grains, that allows identifying the slip traces of sliding systems after tensile tests and thus estimate their CRSS ratios with lesser effects of crystallographic texture. T1-UFG, T1-FG and T1-SD are characterized by ultra fine grains, fine grains and standard grains microstructures respectively and the same crystallographic texture (all are strongly textured). Consequently, the effects of the grain size on the activation of sliding systems and therefore optimization of their absolute CRSS in relationship with the grain size can be addressed. The morphology as well the crystallographic texture of these Ti-6Al-4V microstructures are illustrated in Fig. 1 and 2.

Table 1: grain size and crystallographic texture of the investigated microstructures of Ti-6Al-4V.

Microstructure	**grain size** (μm)	**Crystallographic texture**
T1-UFG	0.6	Strong
T1-FG	3	Strong
T1-SD	7.5	Strong
T2-SD	7.5	Weak

Tensile test until 5% of strain was performed for T2-SD. Then, experimental slip traces were then observed by Scanning Electron Microscopy (SEM) and identified using the ori-

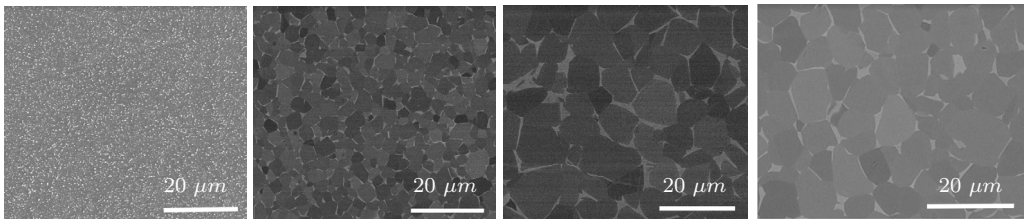

Figure 1: Ti-6A-4V microstructures of (a)T1-UFG, (b) T1-FG, (c) T1-SD and (d) T2-SD

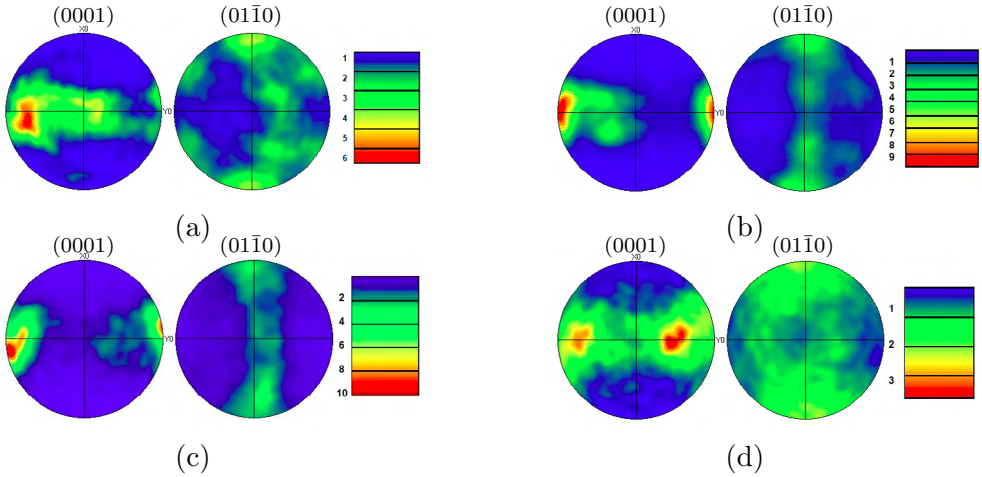

Figure 2: (0001) and $\{10\bar{1}0\}$ pole figures of different Ti-6Al-4V microstructures (a) T1-UFG, (b) T1-FG, (c) T1-SD, (d) T2-SD.

entation data (i.e. Euler angles) provided by Electron Backscatter Diffraction (EBSD) analysis and `ImageJ` software. The prediction of the most likely slip systems to be activated was carried out by comparing the results from theoretical slip trace with the experimental results. An algorithm was developed to calculate the Schmid factor and slip trace angle of each theoretical slip system relative to the orientation of a single grain. The activation of the actual and theoretical slip system was then recorded as a function of slip system type and the Schmid factor as shown in Tab. 2. 3.

230 grains were analyzed, 134 of them present a slip traces (58%). The Schmid factor of 3 basal $\langle a \rangle$, 3 prismatic $\langle a \rangle$ and 6 pyramidal $\langle c+a \rangle$ systems was computed for each yield grain. 1608 values are therefore determined (Tab. 3). The statistical procedure proposed by Li et al. [6] was adapted in this paper for identifying the CRSS ratios. The experimental observed slip systems were compared with those given by the theory by dividing each pair in Tab. 2 designed by O_{ij} with the corresponding theoretical pair T_{ij} in Tab. 3 as:

$$R_{ij} = O_{ij}/T_{ij} \tag{1}$$

Where i is the slip systems type, it can be: basal $\langle a \rangle$ $(i = 1)$, prismatic $\langle a \rangle$ $(i = 2)$ and

Table 2: Distribution of experimental observed slip systems O_{ij} as function of their schmid factor

Schmid factor	**Basal** $\langle a \rangle$ **(34%)**	**Prismatic** $\langle a \rangle$ **(44%)**	**Pyramidal** $\langle c+a \rangle$ **(22%)**
0-0.05	1	3	0
0.05-0.10	0	5	0
0.10-0.15	1	5	0
0.15-0.20	0	8	0
0.20-0.25	3	7	1
0.25-0.30	3	9	2
0.30-0.35	4	8	4
0.35-0.40	7	10	6
0.40-0.45	13	10	9
0.45-0.50	28	12	16

pyramidal $\langle c+a \rangle$ $(i = 3)$ and j is the Schmid factor range $(1 \leq j \leq 10)$. The obtained results are presented in Tab. 4. If all the slip systems represented in Tab. 2 are actually

Table 3: Distribution of theoretical slip systems T_{ij} as function of their Schmid factor for 134 yield grains

Schmid factor	**Basal** $\langle a \rangle$	**Prismatic** $\langle a \rangle$	**Pyramidal** $\langle c+a \rangle$
0-0.05	43	75	114
0.05-0.10	39	65	108
0.10-0.15	55	57	102
0.15-0.20	39	42	88
0.20-0.25	29	31	72
0.25-0.30	45	35	73
0.30-0.35	33	33	66
0.35-0.40	45	24	68
0.40-0.45	30	24	67
0.45-0.50	44	16	46

activated in the experiment, the value of each pair R_{ij} in Tab. 4 would be 1. However, the activation of slip systems depends on their Schmid factor. Thus, slip systems with small Schmid factor is less likely to be activated than those with large Schmid factor (Tab. 4). By comparing the ratios R_{ij} of the same row in Tab. 4, it can be clearly observed that the critical resolved shear stress (CRSS) is different from a family to another. The representation of these ratios follows a cubic distribution (See Fig. 3), thus, using this table as a reference, the theoretical values presented in Tab. 3 can be formulated with cubic weighting function [6] as:

$$w_{ij} = T_{ij} \times ((j-1)/9)^3 \tag{2}$$

This function allowed to reduce the values of theoretical sliding having a small Schmid factor. In this step, the effects of crystallographic texture were eliminated. However,

Table 4: Distribution of the ratios R_{ij} between observed and theoretical slip systems

Schmid factor	**Basal** $\langle a \rangle$	**Prismatic**$\langle a \rangle$	**Pyramidal**$\langle c+a \rangle$
0-0.05	0.023	0.04	0
0.05-0.10	0	0.077	0
0.10-0.15	0.0181	0.087	0
0.15-0.20	0	0.1904	0
0.20-0.25	0.10	0.22	0.014
0.25-0.30	0.067	0.027	0.028
0.30-0.35	0.121	0.29	0.061
0.35-0.40	0.56	0.417	0.089
0.40-0.45	0.43	0.42	0.13
0.45-0.50	0.64	0.75	0.34

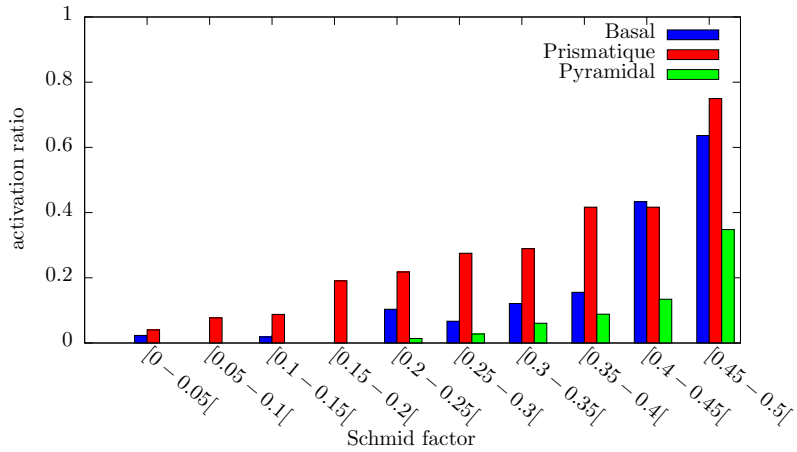

Figure 3: Evolution of the ratios R for each slip system type as function of Schmid factor range.

the CRSS of the different sliding types is not yet taken into consideration. The results obtained using Eq. 2 are presented in Tab. 5.

The probability density function of each pair of Tab. 5 is given as:

$$p_{ij} = \frac{w_{ij}}{\sum_{i=1}^{3} \sum_{j=1}^{10} w_{ij}} \tag{3}$$

Hence, the prediction of the number of slip systems which can be observed experimentally was possible. It can be performed by multiplying the obtained probability density function by the total number N of observed sliding O_{ij} presented in Tab. 2 as:

$$E_{ij} = p_{ij} \times N \tag{4}$$

The results were then reported for each pair (slip system-Schmid factor) in Tab. 6.

It was observed that the results of the expected slip systems (Tab. 6) were significantly different from those experimentally observed (Tab. 2). Noted that until this step, the

CRSSs are always assumed the same for all the slip systems types. The next step of this methodology consists to minimize the difference between the observed and expected values by identifying the CRSSs ratios. The expected number of slip systems E_{ij} can be

Table 5: Distribution of weighted theoretical slip systems w_{ij} for the 134 yielding grains

Schmid factor	**Basal** $\langle a \rangle$	**Prismatic** $\langle a \rangle$	**Pyramidal** $\langle c+a \rangle$
0-0.05	0	0	0
0.05-0.10	0.053	0.089	0.1481
0.10-0.15	0.603	0.625	1.119
0.15-0.20	1.445	1.556	3.259
0.20-0.25	2.546	2.721	6.320
0.25-0.30	7.716	6.001	12.517
0.30-0.35	9.778	9.778	19.555
0.35-0.40	21.173	11.292	31.994
0.40-0.45	21.069	16.855	47.059
0.45-0.50	44	16	46

thus modified by introducing the CRSS of each type i designated by τ_i^c as:

$$M_{ij} = \frac{a}{\tau_i^c} E_{ij} \tag{5}$$

Where a is a unknown parameter, it can be found if at least one of the $CRSS_i$ is determined. However, in the most of previous investigations, only the relative CRSSs were identified (see [6]). The optimal values of CRSS can be estimated by minimizing the

Table 6: Distribution of the expected slip systems E_{ij} as function of their Schmid factor

Schmid factor	**Basal**$\langle a \rangle$	**Prismatic**$\langle a \rangle$	**Pyramidal**$\langle c+a \rangle$
0-0.05	0	0	0
0.05-0.10	0.0274	0.0457	0.0759
0.10-0.15	0.309	0.320	0.573
0.15-0.20	0.740	0.797	1.671
0.20-0.25	1.305	1.395	3.241
0.25-0.30	3.956	3.077	6.418
0.30-0.35	5.013	5.013	10.027
0.35-0.40	10.857	5.790	16.406
0.40-0.45	10.804	8.643	24.129
0.45-0.50	22.562	8.204	23.588

cumulative error Er between the number of observed O_{ij} slip systems and the expected ones M_{ij}. This can be performed using the square difference equation as:

$$Er = \sqrt{d^2(O_{ij}, M_{ij})} = \sqrt{\sum_{i=1}^{3} \sum_{j=1}^{10} (O_{ij} - M_{ij})^2} \tag{6}$$

By replacing M_{ij} with $\frac{a}{\tau_i^c}E_{ij}$, Er can be rewritten:

$$Er = \sqrt{\sum_{i=1}^{3}\sum_{j=1}^{10}(O_{ij} - \frac{a}{\tau_i^c}E_{ij})^2} \tag{7}$$

The optimal τ_i^{*c} was therefore obtained by solving the first-order derivative equation as:

$$\frac{\partial Er}{\partial \tau_i^c} = 0 \rightarrow \tau_i^{*c} = a\frac{\sum_{j=1}^{10}(E_{ij})^2}{\sum_{j=1}^{10}O_{ij}E_{ij}} \tag{8}$$

The unknown parameter a vanishes by calculating the ratio between τ^{*c}. The relative CRSS are therefore given by:

$$\frac{\tau_1^{*c}}{\tau_2^{*c}} : \frac{\tau_2^{*c}}{\tau_2^{*c}} : \frac{\tau_3^{*c}}{\tau_2^{*c}} = 1.36 : 1 : 2.84 \tag{9}$$

for basal $\langle a\rangle$:prismatic $\langle a\rangle$:pyramidal $\langle c+a\rangle$ respectively. The obtained results were compared with some results found in the literature (Tab. 7).

Table 7: Estimated relative CRSS in comparison with those found in the literature for Ti-6Al-4V titanium alloy.

Basal $\langle a\rangle$	Prismatic $\langle a\rangle$	Pyramidal $\langle a\rangle$	Reference
1.36	1	2.84	the present study
1.05	1	1.68	[10]
1-1.5	1	3-5	[8]
0.93-1.3	1	1.1-1.6	[5]
1.43	1	4.23	[9]

In order to investigate the effects of grain size on the CRSS, tensile tests were performed until the beginning of plastic behavior (about 1 to 1.3% of total strain) for all T1-UFG, T1-FG and T1-SD microstructures presented in Tab. 1. A multi-scale numerical optimization of absolute CRSS was then carried out using the obtained CRSS ratios, the tensile curves, the crystallographic orientations of 500 grains, a local behavior model and scale transition rules available in `Z_optim` library as summarized in Fig. 4. Noted that the same procedure was repeated for each microstructure. The local behavior model of Méric-Cailletaud [11]was used. It gives a phenomenological description of each slip system behavior. In this model, the slip strain rate $\dot{\gamma}^s$ of system s is given as a form of power function of the resolved shear stress τ^s as:

$$\dot{\gamma}^s = \dot{v}^s sign(\tau^s - \chi^s) \tag{10}$$

With:

$$\dot{v}^s = \left\langle \frac{|\tau^s - \chi^s| - r^s}{K} \right\rangle^n \tag{11}$$

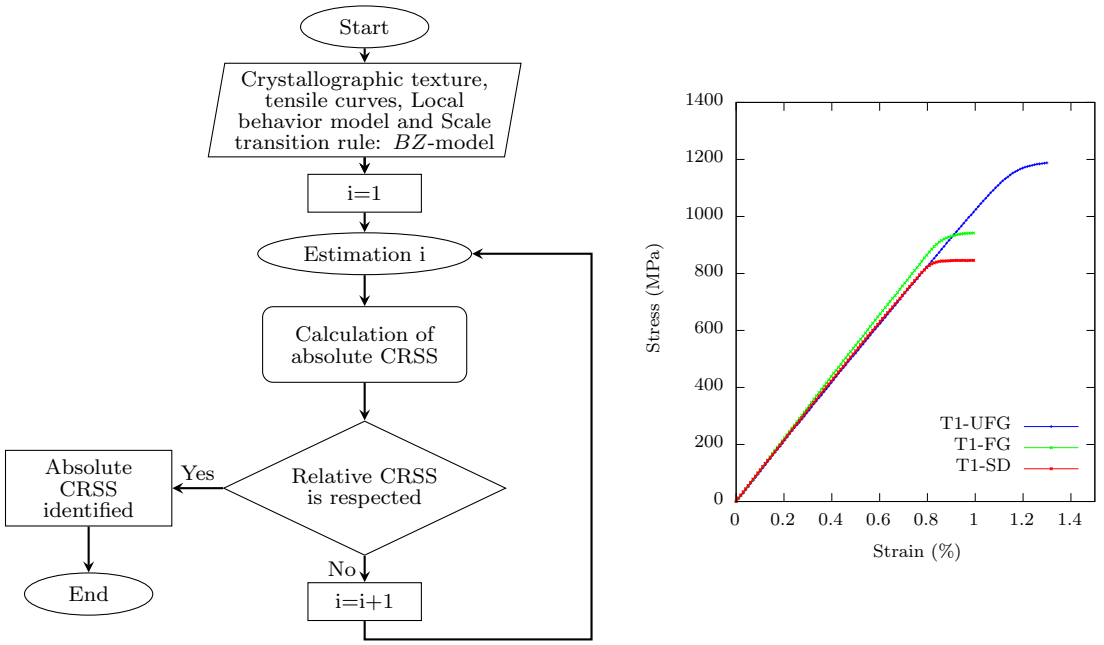

Figure 4: Methodology for optimizing the absolute CRSS: (a) the followed procedure uses a local behavior model of Méric-Cailletaud [11], Berveiller-Zaoui model [12] (BZ) for transition Scale and model parameters of Dick et al [10]. (b) The experimental tensile curves.

Where χ^s and r^s are the kinematic and the isotropic hardening variables of slip system s respectively, τ^s is the resolved shear stress of systems s , K and n characterize the material viscosity. The isotropic hardening r^s was considered constant and equal to the absolute Critical Resolved Shear Stress CRSS (τ_c^s).

$$r^s = \tau_c^s \tag{12}$$

Moreover, the hardening nonlinearity can be expressed by the nonlinear kinematic hardening of slip systems according to the Armstrong-Frederick equation: [13]:

$$\chi^s = C\alpha^s \tag{13}$$

With:

$$\dot{\alpha}^s = \dot{\gamma}^s - d\alpha^s\dot{\chi}^s \tag{14}$$

Where α^s is a state variable describing the evolution of kinematic hardening in slip system s. C and d are the material parameters. The kinematic hardening and the viscosity parameters determined by Dick et al. [10] were used. Berveiller-Zaoui model [12] (BZ) was chosen as a scale transition rule for the identification procedure. For this model, the localization of the stress tensor is given by Eq. (15):

$$\sigma^g = \Sigma + 2\mu\alpha(1-\beta) : (E^p - \varepsilon^{g,p}) \tag{15}$$

with:

$$\frac{1}{\alpha} = 1 + \frac{3}{2}\mu\frac{E^p_{eq}}{\Sigma_{eq}} \tag{16}$$

and

$$\beta = \frac{2(4-5\nu)}{15(1-\nu)} \tag{17}$$

where σ^g and Σ are respectively the stresses at mesoscopic (grain) and macroscopic (global) scales, $\varepsilon^{g,p}$ and E^p are respectively the local and global plastic strain, ν is the Poisson ratio, μ the shear modulus and ρ stands for a non linear accommodation parameter whose formulation is a function of the Von-Mises equivalent inelastic strain E^p_{eq} and stress Σ_{eq} at the macroscopic scale.

The comparison between the identification results of CRSS provided by the Meric-Cailletaud model using the Berveiller-Zaoui transition rule and the experimental tensile results is illustrated in Fig. 5.

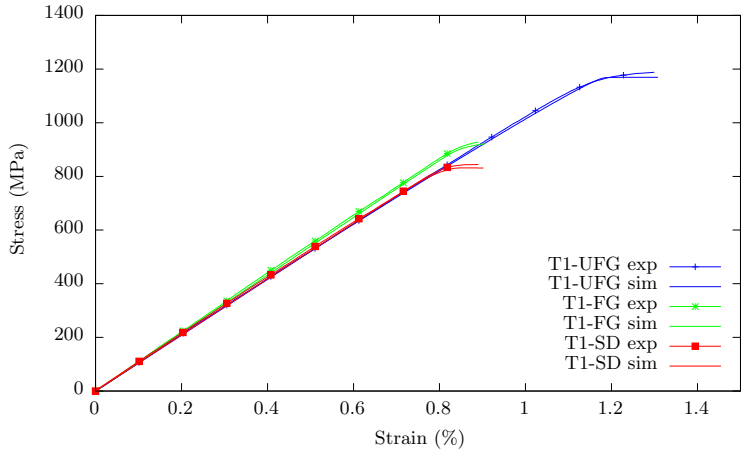

Figure 5: Comparison between experimental strain-stress curves and those provided using the identified CRSS and BZ transition scale rule for each Ti-6Al-4V microstructure

For each Ti-6Al-4V microstructure, the absolute CRSSs of slip systems types were reported in Tab. 8. they can be then formulated as a function of the inverse square root of the average grain size (Fig. 6) according to the Hall-Petch relationship [14, 15]:

$$\tau^c_i = K^{hp}_i \frac{1}{\sqrt{D}} + \tau^0_i \tag{18}$$

Where K^{hp}_i and τ^0_i are the Hall Petch slope and the friction lattice stress of slip systems type i respectively and D is the average grain size.

The local Hall-Petch slope was found to be 146, 114 and 225 $MPa.m^{-1/2}$ for basal $\langle a \rangle$, prismatic $\langle a \rangle$ and pyramidal $\langle c+a \rangle$ systems respectively. The increase of grain size leads to decrease the CRSS and therefore facilitates the accommodation of the plastic strain in coarse grains. The Hall-Petch slope of pyramidal $\langle c+a \rangle$ systems is very high compared

Table 8: Absolute Critical Resolved Shear Stress (CRSS).

Material	**Absolute CRSS (MPa)**		
	Basal	Prismatic	Pyramidal
T1-UFG	390	290	790
T1-FG	320	240	570
T1-SD	240	170	580
T1-SD	240	170	580

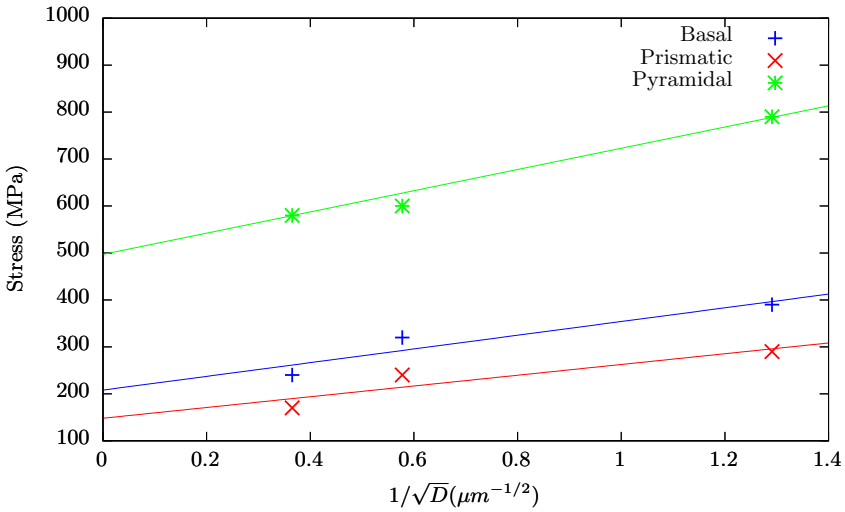

Figure 6: Effect of grain size on CRSS of slip systems types

with those of prismatic and basal systems which can lead to a significant decrease of pyramidal $\langle c+a \rangle$ CRSS in large grains.

3 CONCLUSIONS

A slip trace analysis followed by a statistical reasoning and a multi-scale numerical optimization were utilized in order to identify the critical resolved shear stress CRSS of basal $\langle a \rangle$, prismatic $\langle a \rangle$ and pyramidal $\langle c+a \rangle$ systems in three microstructures of Ti-6Al-4V alloy. A significant role of grain size was shown; by increasing the average grain size, the CRSS decreases . This effect was correctly modeled by the Hall-Petch relationship. Moreover, the dependence of CRSS on grain size varies from a type of sliding to another. Pyramidal $\langle c+a \rangle$ systems type shows the highest Hall-Petch slope, this leads to a significant decreasing of pyramidal CRSS in large grains which justifies its activation although its relative CRSS is more than 2.5 times of prismatic CRSS.

Acknowledgments

The authors wish to thank French Occitanie Region for the growth of research activities at the IMT-Mines Albi and Figeac IUT. The authors would also like to gratefully

acknowledge the NHK spring company-Japan (https://www.nhkspg.corjp/eng/) for its support by providing the material used in the contribution.

REFERENCES

[1] M. Philippe, E. Bouzy, and J. Fundenberger, "Textures and anisotropy of titanium alloys," *Materials Science Forum*, vol. 273-275, pp. 511–522, 1998.

[2] G. Gilles, W. Hammami, V. Libertiaux, O. Cazacu, J. Yoon, T. Kuwabara, A. Habraken, and L. Duchne, "Experimental characterization and elasto-plastic modeling of the quasi-static mechanical response of TA6V at room temperature," *Solids and Structures*, vol. 48, pp. 1277–1289, 2011.

[3] W. Tirry, F. Coghe, S. Bouvier, M. Gasperini, L. Rabet, and D. Schryvers, "A multiscale characterization of deformation twins in Ti-6Al-4V sheet material deformed by simple shear," *Materials Science and Engineering A*, vol. 527, pp. 4136–4145, 2010.

[4] J. Williams, R. Baggerly, and N. Paton, "Deformation behavior of HCP TiAl alloy single crystals," *Metallurgical and Materials Transactions A*, vol. 33, pp. 837–850, 2002.

[5] J. M. Perilla and J. Sevillano, "Two-dimensional sections of the yield locus of a Ti-6Al-4V alloy with a strong transverse_type crystallographic a-texture," *Materials Science and Engineering A*, vol. 201, pp. 103–110, 1995.

[6] H. Li, D. Mason, T. Bieler, C. Boelert, and M. Crimp, "Methodology for estimating the critical resolved shear stress ratios of a-phase Ti using EBSD-based trace analysis," *Acta Materialia*, vol. 61, pp. 7555–7567, 2013.

[7] D. Dunst and H. Mecking, "Analysis of experimental and theoretical rolling textures of two-phase titanium alloys," *Zeitschrift fuer Metallkunde*, vol. 87, pp. 498–507, 1996.

[8] J. Mayeur and D. McDowell, "A three-dimensional crystal plasticity model for duplex Ti6Al4V," *Plasticity*, vol. 23, pp. 1457–1485, 2007.

[9] S. Semiatin and T. Bieler, "Effect of texture and slip mode on the anisotropy of plastic flow and flow softening during hot working of Ti6Al4V," *Metallurgical and Materials Transactions A*, vol. 32, pp. 1787–1799, 2001.

[10] T. Dick and G. Cailletaud, "Fretting modelling with a crystal plasticity model of Ti6Al4V," *Computational Materials Science*, vol. 38, pp. 113–125, 2006.

[11] L. Méric, P. Poubanne, and G. Cailletaud, "Single crystal Modeling for Structural Calculations: Part 1model presentation," *Engineering Materials and Technology*, vol. 113, pp. 162–170, 1991.

[12] M. Berveiller and A. Zaoui, "An extension of the self-consistent scheme to plastically-flowing polycrystals," *Mechanics and Physics of Solids*, vol. 26, pp. 325–344, 1978.

[13] C. Frederick and P. Armstrong, "A mathematical representation of the multiaxial bauschinger effect," *Materials high temperature*, vol. 24, pp. 1–26, 2007.

[14] E. Hall, "The deformation and ageing of mild steel: III discussion of results," *Proceedings of the Physical Society B*, vol. 64, pp. 747–753, 1951.

[15] N. Petch, "The cleavage strength of polycrystals," *the Iron and Steel Institute*, vol. 174, pp. 25–28, 1953.